PAPER • OPEN ACCESS

Probing shock dynamics inside micro-wire targets after high-intensity laser irradiation using small angle x-ray scattering of a free-electron laser

IOP Publishing New J. Phys. 25 (2023) 103036 https://doi.org/10.1088/1367-2630/acfab5

New Journal of Physics
The open access journal at the forefront of physics

Deutsche Physikalische Gesellschaft DPG
IOP Institute of Physics

Published in partnership with: Deutsche Physikalische Gesellschaft and the Institute of Physics

OPEN ACCESS

RECEIVED
22 March 2023

REVISED
16 August 2023

ACCEPTED FOR PUBLICATION
18 September 2023

PUBLISHED
19 October 2023

PAPER

Probing shock dynamics inside micro-wire targets after high-intensity laser irradiation using small angle x-ray scattering of a free-electron laser

Thomas Kluge[1,*], Michael Bussmann[1], Eric Galtier[2], Siegfried Glenzer[2], Jörg Grenzer[1], Christian Gutt[3], Nicholas J Hartley[2], Lingen Huang[1], Alejandro Laso Garcia[1], Hae Ja Lee[2], Emma E McBride[2,4], Josefine Metzkes-Ng[1], Motoaki Nakatsutsumi[4], Inhyuk Nam[2,7], Alexander Pelka[1], Irene Prencipe[1], Lisa Randolph[3,8], Martin Rehwald[1,5], Christian Rödel[2,6], Melanie Rödel[1], Toma Toncian[1], Long Yang[1], Karl Zeil[1], Ulrich Schramm[1,5] and Thomas E Cowan[1,5]

[1] Helmholtz-Zentrum Dresden-Rossendorf, Bautzner Landstraße 400, Dresden 01328, Germany
[2] SLAC National Accelerator Laboratory, 2575 Sand Hill Rd, Menlo Park, CA 94025, United States of America
[3] Universität Siegen, Adolf-Reichwein-Straße 2, Siegen 57068, Germany
[4] European XFEL, Holzkoppel 4, 22869 Schenefeld, Germany
[5] Technical University Dresden, 01069 Dresden, Germany
[6] University of Applied Sciences Schmalkalden, Blechhammer 6-9, Schmalkalden 98574, Germany
[7] Now with Pohang Accelerator Laboratory, Pohang, Gyeongbuk 37673, Republic of Korea
[8] Now with European XFEL, Holzkoppel 4, 22869 Schenefeld, Germany
[*] Author to whom any correspondence should be addressed.

E-mail: t.kluge@hzdr.de

Keywords: plasma, SAXS, XFEL, laser, proton acceleration

Abstract

In this paper, we present an experiment that explores the plasma dynamics of a 7 μm diameter carbon wire after being irradiated with a near-relativistic-intensity short pulse laser. Using an x-ray free electron laser pulse to measure the small angle x-ray scattering signal, we observe that the scattering surface is bent and prone to instability over tens of picoseconds. The dynamics of this process are consistent with the presence of a sharp, propagating shock front inside the wire, moving at a speed close to the hole boring velocity or that expected from a thermal shock at a few tens of Mbar.

1. Introduction

Modern laser technology allows the generation of ultra-intense optical light, compressed to a few femtoseconds and focused to a few micron spot sizes leading to intensities exceeding the threshold for relativistic electron motion of $\sim 10^{18}\,\mathrm{W\,cm^{-2}}$. When a laser pulse is focused on a solid surface at these intensities, the atoms at the surface are ionized and a dense plasma is created. The laser field interacts with electrons within a skin depth of a few tens of nanometers and can compress the surface and accelerate electron and ions to several MeV. The interaction of such high intensity lasers with solids has attracted considerable interest with the prospect of creating bright and compact particle accelerators [1] and gamma-ray sources [2].

Several physical processes occur before or after the laser pulse on a picosecond to nanosecond time scale leading for example to thermalization, diffusion, compression and ablation [3]. These processes generally take place in the regime of coupled plasmas, where atomic-scale collisions still play a role. Processes on the sub-picosecond or even sub-femtosecond scale on the other hand usually are collective, giving rise to complex phenomena and waves. One important aspect is the generation of a multitude of instabilities, influencing for example the coupling of the laser to the plasma, particle transport, and heating of the target. So far, such surface plasma dynamics have been widely investigated using femtosecond optical laser pulses [4], whereby various surface-sensitive methods based on optical shadowgraphy [5–7], interferometry [8], and spectroscopy [9–11] have been applied. However, optical probes can only penetrate

the plasma up to their critical density, i.e. a fraction of the solid density, and so cannot directly give access to the dynamics inside the solid density region.

X-ray diffraction can be employed to resolve physical processes above the critical density, such as for example non-thermal melting [12], coherent lattice vibrations [13], and ultrafast phase transitions [14]. Recently, x-ray pulses from x-ray free electron lasers (XFELs) have been applied to investigate laser produced plasmas with femtosecond temporal resolution. Small-angle femtosecond x-ray scattering (SAXS) has revealed density gradients of expanding solid-density plasmas with nanometer spatial and few femtosecond temporal resolution [15–17], transient nano-jet emission from grating surfaces [17], as well as ultra-fast heating and ionization [18, 19].

Here we use SAXS to study the dynamics inside solid density wires that turn into plasmas after high-intensity short-pulse laser irradiation. Our experimental data shows that the scattering surface is bent by a few microns and prone to instability development also on the scale of a few microns over the course of tens of picoseconds. The dynamics of this process are consistent with a sharp, propagating compression (shock) front inside the wire. With the novel SAXS method we measure the tilt angle of this front and observe that it is moving forward with a speed of up to $0.1\,\mu\mathrm{m\,ps^{-1}}$, which is close to that expected from a thermal shock at a few tens of Mbar or from a shock launched by the hole boring (HB) pressure.

2. Experimental setup

We report on an experiment probing the plasma dynamics of a $7\,\mu$m diameter carbon wire (density $2.25\,\mathrm{g\,cm^{-3}}$) after the irradiation with the near-relativistic high-intensity (HI) titanium:sapphire short-pulse near-infrared (wavelength 800 nm) laser at the Matter in Extreme Conditions (MEC) endstation at the linear coherent light source (LCLS) XFEL. The HI laser pulse duration was 83 fs and the spot size at full width half maximum (FWHM) was $w_x \simeq 30\,\mu$m and $w_y \simeq 16\,\mu$m in horizontal and vertical direction, respectively. The laser pulse energy was measured to be up to 1 J before compression. With 46% transmission to the target and 22% of the energy being in the FWHM area, the peak intensity on target can be calculated to approx. $5 \times 10^{17}\,\mathrm{W\,cm^{-2}}$, equivalent to a normalized laser strength amplitude of $a_0 \cong 0.5$. The XFEL pulse had a diameter of 5–10 μm and pulse duration of 40 fs, both at FWHM. The x-ray photon energy was 8 keV, with approximately $N_0 = 10^{11}$ photons per pulse (the exact number on target varies from shot to shot due to different absorbers). Temporal synchronization between the HI short-pulse laser and LCLS XFEL pulse was achieved with a precision of 120 fs rms.

The carbon wire targets were irradiated under normal incidence by both the pump and the probe pulse, which were also perpendicular to each other, see figure 1. For reasons detailed below, the XFEL axis was vertically offset by approximate $20\,\mu$m along the wire towards the top.

In the following, we present a series of shots on these wires, varying the pump laser intensity between 50% and 100% (i.e. between $3.5 \times 10^{17}\,\mathrm{W\,cm^{-2}}$ and $7 \times 10^{17}\,\mathrm{W\,cm^{-2}}$), and the probe delay Δt between 0 and 80 ps. We measure the SAXS signal with an PIXIS2048 x-ray detector with $13\,\mu$m pixel size that was positioned 1.4 m behind the target. In this configuration, the signal is given in Born approximation (i.e. phase contrast only) by the Fourier transform of the electron density, $I(\boldsymbol{q}) \propto |\mathrm{FT}(n(\boldsymbol{r}))|$, where $q = |\boldsymbol{k}_0 - \boldsymbol{k}'|$) is the scattering vector defined by the difference between the incoming XFEL wave vector $\boldsymbol{k}_0$ and the scattered wave vector $\boldsymbol{k}'$. Here, we only expect two streaks perpendicular to the wire surface, the interference pattern of scattered waves from the wire front and rear surface (i.e. $q = 2\pi/7\,\mu\mathrm{m} \simeq 9 \times 10^{-4}\,\mathrm{nm^{-1}}$) cannot be resolved with the detector resolution of at least 2 detector pixels due to the finite point spread function and XFEL focus size (one pixel is $\Delta q = k_0 \times 13\,\mu\mathrm{m}/1.4\,\mathrm{m} \simeq 4 \times 10^{-4}\,\mathrm{nm^{-1}}$). The setup we employ here enables the study of a multitude of relevant physics following the relativistic laser irradiation [15], through the analysis of the change of the scattering streak's signal intensity and slope, orientation, and structure, as discussed in the following.

3. SAXS method

First, we would like to extract the temporal evolution of the plasma expansion, as we demonstrated before on grating targets [17]. Similar to the Debye–Waller analysis for thermal motion of particles, we can replace the displacement of scatterers due to thermal motion with the displacement of the plasma due to non-thermal melt/expansion into vacuum. The expansion scale σ can then simply be derived from the exponential roll-off of the scattering signal at large scattering angles [16, 17]

$$I(q) \propto q^{-r} \exp\left(-q^2\sigma^2\right) \tag{1}$$

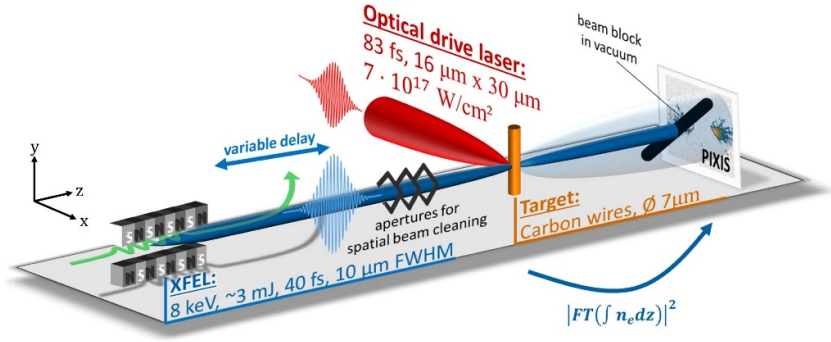

(a) Setup

(b) Effect of XFEL vertical offset

Figure 1. (a) Sketch of the setup of the experiment, not to scale. The high intensity short pulse pump laser irradiates the wire at normal incidence, an XFEL pulse probes the plasma under 90° incidence. The detector was positioned at a distance to the target of 1.4 m. The XFEL was vertically off-centered, effecting the signal: (b) the XFEL scattering streak (blue line) is assumed to stand perpendicular on the scattering surface of the wire. The scattering surface can be (i) the forward ablated surface, (ii) the hole boring (shock) front, (iii) the rear surface rare faction wave, (iv) the ablated rear surface, or a mechanically bent foil. Due to the measured orientation of the streak (see figures 2 and 3, (i), (iii)) can be ruled out.

where r depends on the geometry of the sample. The exponent r is expected for flat surfaces to be in the range of 2–4, e.g. $r = 2$ for a cuboid, $r = 3$ for a cylinder and $r = 4$ for a sphere [20], or $r = 3$–4 for a fractally rough surface [21]. The exponential term is the Debye–Waller factor.

Secondly, we can expect the scattering streak of the wire to tilt if the wire is being deformed by the laser. As depicted in figure 1(b), this can in principle happen due to (i) ablation into vacuum at the front following the thermal pressure set up by laser accelerated electrons or the bulk electrons heated by return current collisions [22, 23]; (ii) a traveling compression (HB or shock) front into the bulk launched by the laser pressure [24, 25] or thermal pressure [26]; (iii) a rarefaction (shock) wave into the wire at the rear surface [27]; (iv) ablation into vacuum at the rear [23].

To determine the relevant mechanisms in the present setup, we employ simulations already published for similar conditions (cp. figure 3 of [19]). The laser and XFEL parameters are the same while only the target material differs, being Si in the simulation instead of the carbon used here. However, the effective scattering length densities $\int n_e \mathrm{d}z$ are essentially the same and the simulations therefore describe also the present case qualitatively. As can be seen in these simulations, over the course of only a few picoseconds the front surface is fully ablated (i.e. order of μm scalelength). Such a diluted surface would not be possible to be detected due to the corresponding Debye–Waller factor that would be close to zero and would suppress the streak signal already at small q, effectively making the streak vanish. Simultaneously, a compression shock wave is launched by the laser pressure (HB), which continues to travel through the target over 10 s of picoseconds as a thermal shock wave with a pressure of $\cong 50$ Mbar. Similar dynamics have been previously reported at slightly higher laser intensity [26]. The shock front velocity is between $0.05\,\mu\mathrm{m\,ps^{-1}}$ (hydro simulation) and $0.1\,\mu\mathrm{m\,ps^{-1}}$ (PIC simulation), i.e. around the theoretical prediction for a thermal shock

$$v_{\mathrm{thermal}}^{\mathrm{shock}} = \sqrt{3P/\rho_0} \cong 0.08\,\mu\mathrm{m\,ps^{-1}} \tag{2}$$

and close to the HB velocity

$$v_{\mathrm{HB}} = c\frac{\Xi}{1+\Xi} \cong 0.09\,\mu\mathrm{m\,ps^{-1}} \tag{3}$$

where the piston parameter for a fully ionized plasma is $\Xi \cong a_0/2\sqrt{m_p n_e/m_e n_c}$, m_i and m_e are the ion and electron mass, respectively, and $n_c = \varepsilon_0 m_e \omega_0^2/e^2$ is the critical density [24]. Hence we can expect the compression wave to break out of the rear surface of the 7 μm thick carbon wire after approx. 70 ps.

Additionally, briefly after the laser irradiation some high energy electrons accelerated by the laser penetrate the full target ballistically, which excites a return current and consequently bulk target heating to some few eV. Hence, the rear surface expands/ablates slightly due to the thermal pressure. Both features, the shock front and the ablating rear surface, as well as the rarefaction wave countering the rear surface expansion, could in principle lead to a signal in form of a streak on our SAXS detector depending on their exact sharpness.

Finally, instabilities in the shock front or the rear surface, respectively, can lead to a break-up of the single wire scattering line into multiple lines, which in the case of a sinusoidal surface modulation would each

reflect a certain orientation of the target normal at the point of inflection. Such instabilities can be, among others, Rayleigh–Taylor like instabilities leading to a surface rippling at relativistic intensities [28–30], filamentation-two-stream instabilities in the target [31, 32] or at the target rear surface [33], Weibel-like instabilities occurring during the plasma propagation in vacuum after laser acceleration [34], or the Z-pinch sausage ($m = 0$) instability (especially at later times after few ps) [35]. The instabilities lead to a growth of initially small density fluctuations to form ripples even on an initially flat target surface.

In the regime relevant for this work, the dominant source of small angle x-ray scattering is coherent elastic Thomson scattering from electrons, but there is also a relevant diffractive contribution by bound-free transition absorption. The latter depends sensitively on the plasma ionization degree, i.e. the plasma temperature.

4. Results

The scattering patterns recorded in this experiment are shown in figure 2 as a function of delay at full laser intensity, and in figure 3 as function of intensity at 40 ps probe delay. For each shot we took two XFEL-only pre-shots as a reference, that we averaged for better statistics. We used this to determine the undriven target normal orientation and verify the surface quality and XFEL overlap. We also took an XFEL-only post-shot after the combined laser-XFEL main-shot, in order to be able to subtract in the pre- and main-shot the parasitic XFEL scattering on the beamstop and other optical components in the beamline. The figures show the background subtracted and normalized signal.

We start the analysis of the streaks by comparing their lengths, i.e the intensity fall-off with scattering angle (i.e. $I(q)$), cf figures 4 and 5. In none of the shots a Debye–Waller like exponential roll-off at large q-values could be observed. Since the q-range with signal above the background is limited in most of the shots to $q < q_{\max} \cong 0.1/\mathrm{nm}^{-1}$, this means that the surface roughness would be less than

$$\sigma_{\max} \simeq \frac{1}{q_{\max}} \simeq 10\,\mathrm{nm}. \tag{4}$$

In reality this value is even much larger since photon number Poisson statistics, background uncertainty, and the uncertainty of r and its fit correlation with σ add considerable fit uncertainty (the latter alone is approx. a factor of 2). This means that in our case due to the low dynamic range limiting us to very small q-value, the Debye–Waller factor cannot be discriminated from unity in all shots. Setting it to 1 in equation (1), the scattering intensity can thus simply be written as

$$I(q) = \frac{a}{q^r} + b \tag{5}$$

where a is the proportionality factor, b comprises the radiation and detector background signal and r should take on values between 2 and 3. We fitted all the streaks with equation (5) and find a value close to $r = 3$ for all cases, see figure 4. This means that in all cases the shape of the scattering front remains that of a cylinder and is not significantly compressed by the laser towards flatter planar geometry. Having found no significant evidence for expansion nor compression, we conclude that the visual impression of shorter or longer streaks is consistent with being primarily due to different signal levels instead of a change of r or σ.

Secondly, we analyze the tilt angle of the streak in the main-shot relative to the pre-shot. Figure 6 shows the tilt angles as a function of delay for full laser intensity (a), and as function of laser intensity at 40 ps delay (b). As described above, there are several mechanisms that in principle can cause a time-varying signal orientation. Some we can exclude based on our measurements by realizing that our XFEL spatial overlap was vertically shifted approx. 20 μm above the laser interaction point (i.e. $>$ 2 FWHM of the XFEL pulse spot size). This is why we only see one streak—the other streak in the opposite direction is simply not in the XFEL field of view. However, this allows us to infer the direction of the tilt of the scattering surface. In the present case, we conclude that the tilt must be in laser forward direction. This means that those processes that cause a density contour tilt towards the laser can be excluded, i.e. front surface plasma expansion and rear surface rarefaction wave, see figure 1(b).

We are left with the possibilities of rear surface tilt of the target due to plasma expansion into vacuum, or a tilt of the front surface by HB or a compression (shock) front traveling forward, cf figure 1(b) (orange lines). To connect the tilt angle of the streak with the plasma electron density contour more quantitative, we adopt a very simple model. We assume that the scattering surface is moving forward with a velocity that depends on the local laser intensity. In particular, the surface longitudinal position as a function of the transverse offset shall be Gaussian with the same FWHM as the laser amplitude focal spot size w_y. Then it

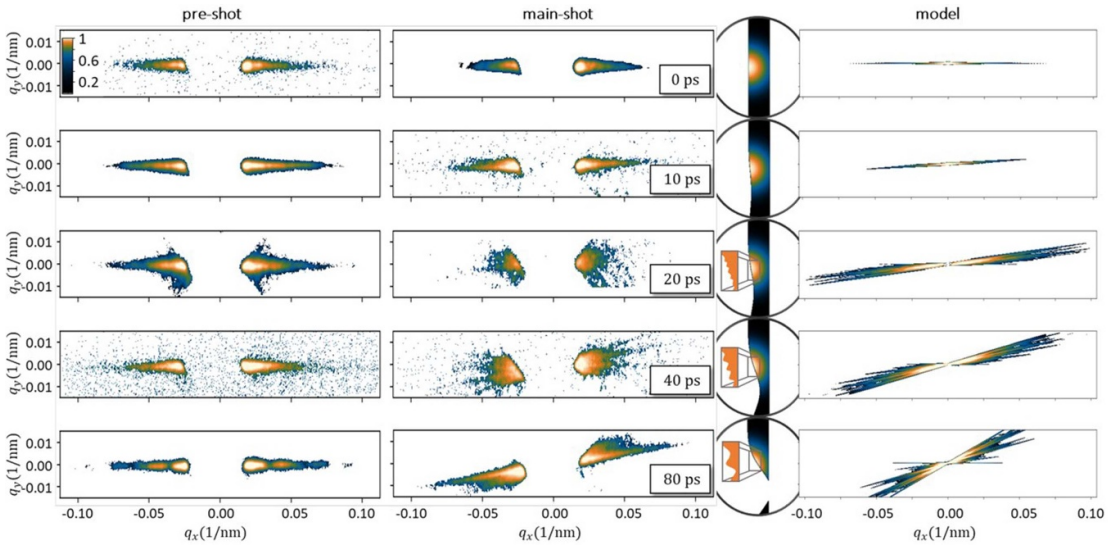

Figure 2. Normalized scattering patterns for different XFEL probe delays (probe comes after pump) at an intensity of $5 \times 10^{17}\,\mathrm{W\,cm^{-2}}$. The right column shows example scattering patterns based on a hole boring model described in (3) and equation (6): the circles depict the example density distribution in real space (multiplied with the XFEL intensity), the right column shows the respective Fourier absolute square signal, for an A in equation (6) of 0 μm, 1 μm, 2 μm, 4 μm, 8 μm (top to bottom). For the cases with delay 20 ps, 40 ps, 80 ps we added a sinosoidal surface structure with 12.5 nm, 25 nm, 50 nm amplitude and 1 μm, 2 μm, 3 μm period, respectively.

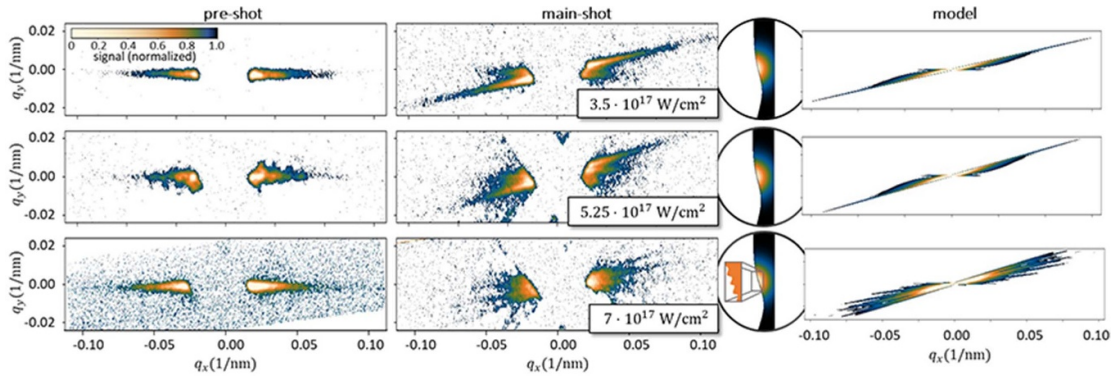

Figure 3. Normalized scattering patterns for different laser intensities. XFEL probe delay was set to 40 ps. The right column shows example scattering patterns based on a hole boring model described in (3) (or an equivalently thermal shock model (2)) and equation (6): the circles depict the example density distribution in real space (multiplied with the XFEL intensity), the right column shows the respective Fourier absolute square signal, for $A = 2.8\,\mu$m (top), 3.5 μm (middle), and 4.0 μm (bottom) in equation (6). As in figure 4, for the case at full intensity we added a sinusoidal surface with 25 nm amplitude and 2 μm period.

can easily be geometrically derived that the target position A along the target normal is connected to the angle α of the normal at the point of inflection (i.e. the tilt angle) via

$$\alpha = \sqrt{e}\frac{w_y}{2\sqrt{\ln 2}A}. \tag{6}$$

From the delay scan of α in figure 6(a) we can then directly obtain the peak forward velocity of $v_f = A/\Delta t \cong 0.1 \pm \mu\mathrm{m\,ps^{-1}}$ until a probe delay of $\Delta t \gtrsim 40$ ps. Obviously at 80 ps delay the measured tilt does not increase anymore. Indeed, extrapolating the forward velocity, we would expect the scattering front to exit the rear of the wire at $\simeq 70$ ps if launched from the front at $t = 0$ (However, one needs to be careful with the interpretation, since we present only single shot results).

From the intensity scan in panel (b) we infer that the forward velocity is proportional to the laser strength parameter a_0, i.e. the square root of the laser intensity, $v_f = c_f a_0$, with a proportionality constant of $c_f \cong 0.19\,\mu\mathrm{m\,ps^{-1}}$.

The forward velocity extracted from both the delay scan and the intensity scan is in remarkable agreement with the HB velocity from equation (3), $v_{\mathrm{HB}} \cong 0.2\frac{\mu\mathrm{m}}{\mathrm{ps}} \times a_0$, and for the full intensity case agrees with the compression front velocity in the aforementioned simulation.

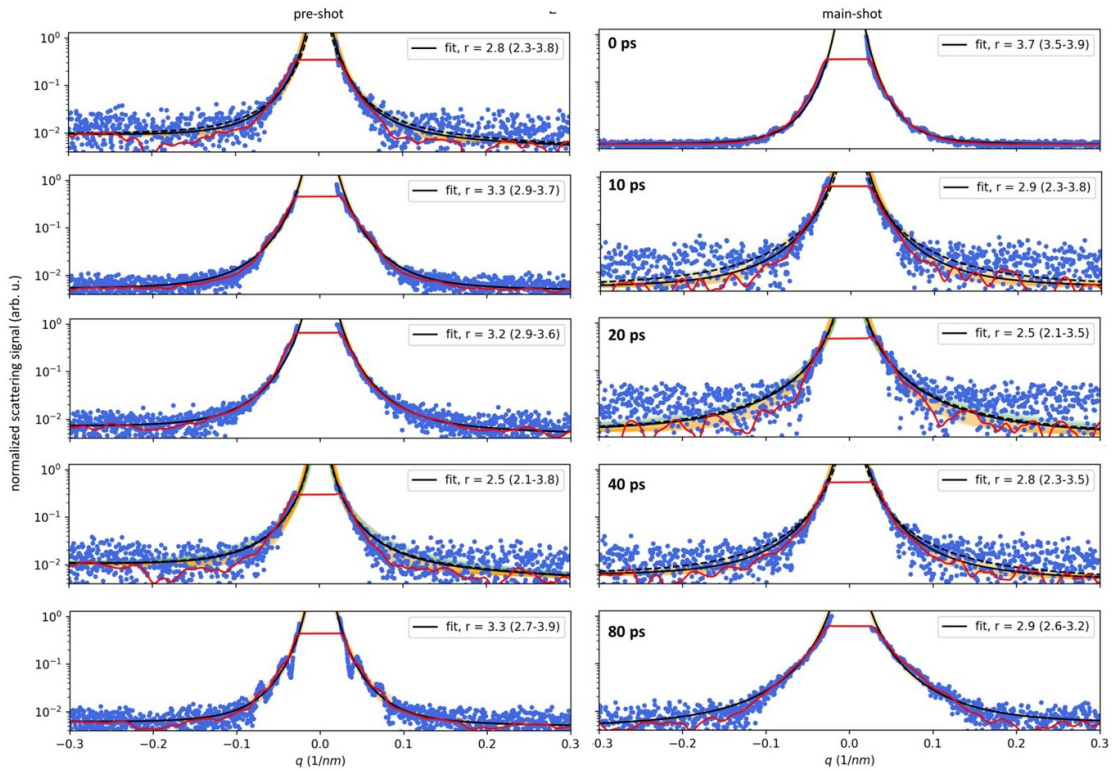

Figure 4. Streak profiles for the scattering patterns shown in figure 2. The red line is the rolling average over 15 px, the black line shows the best fit with the fitted exponent r and its confidence interval (1σ) given in the respective legend. The black dashed line shows the best fit with $r < 2.5$ which is indistinguishable from the black solid line in most cases, to demonstrate how insensitive the fits are with respect to r. The small orange shaded area is the error of the fit.

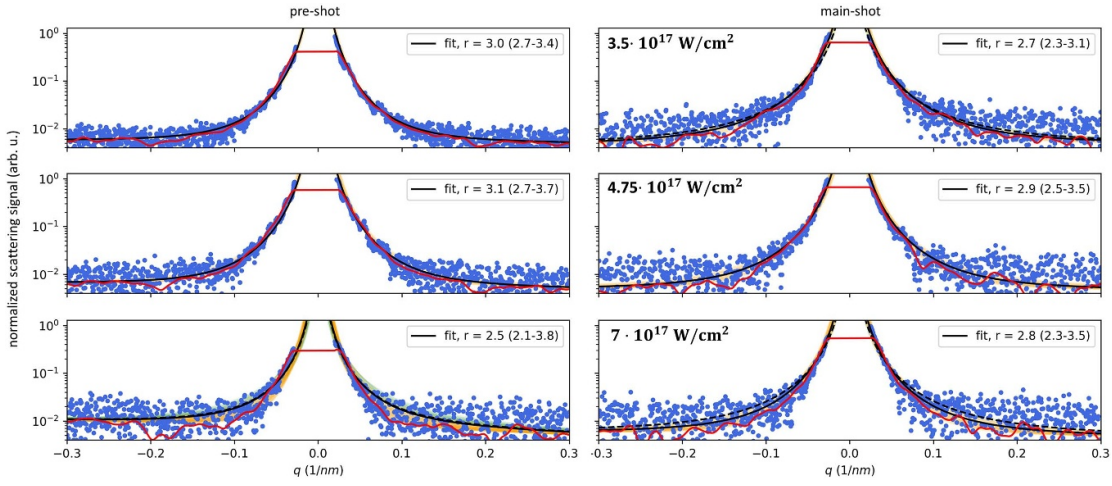

Figure 5. Same as figure 4 but for the streak profiles of the scattering patterns shown in figure 3.

Finally, we point out that the tilted streak transitions into a set of multiple streaks at full intensity after 20 ps. This is indicative for a modulation of the scattering surface. This filamentation starts around 20 ps, is most visible at 40 ps and is not visible at 80 ps after the laser irradiation as strong anymore, though there is still a faint second streak visible. Potentially the instability is still present, but its spatial frequency decreased so that the field of view of the XFEL comprises less filaments. The growth of the instability apparently continues, as the angular spread between the streaks at larger delay values is larger than at earlier times, i.e. the modulation depth seems to be increasing with time. In most shots we additionally see remnants of the streak in horizontal direction, perpendicular to the undriven wire surface. We believe that this is primarily due to scattering of the outer wings of the XFEL spot at the rear surface or vertical distant, unperturbed regions.

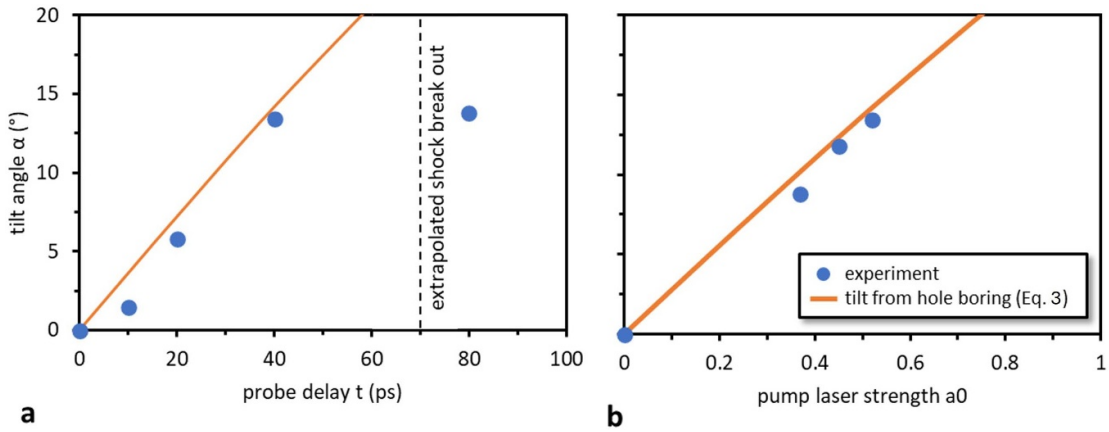

Figure 6. Tilt angle of the streak as a function of probe delay at full pump laser intensity (a) and as a function of pump laser intensity at 40 ps probe delay (b) (blue points), compared to a surface bending forward proportionally to the hole boring velocity computed with the local laser intensity following its transverse Gaussian shape (orange lines).

5. Conclusions

In the experiment presented above we have employed SAXS to measure the target solid density response upon HI laser irradiation. We interpret our measurements with scattering at a compression front inside the target after it detached from the laser radiation pressure accelerated front surface. This follows from the following arguments: First, the simulation in [19] that predict a compression shock front persisting over 10 s of ps. Secondly, the front and rear surface are expected to quickly smooth out due to plasma expansion, so that the streak cannot originate from the ablated wire surfaces. The tilt angle orientation of the measured SAXS streaks that indicates a forward deformation of the scattering surface, i.e. we can exclude the rear surface rarefaction wave. Rather, it is in agreement with a laser compression front following the lateral laser intensity shape. Moreover, the change of the tilt angle as a function of probe delay and pump intensity is in agreement with the HB velocity scaling. Surprisingly, apparently the scattering surface remains quite sharp over many picoseconds, since the observed streak lengths did not change.

At full laser intensity we observe the streak to filament at a probe time 20 ps after HI irradiation. The number of visible streaks then decreases and the distance between streaks seems to increase between 20 ps to 80 ps. This indicates that if the signal was due to a sinusoidal-like modulation of the scattering surface, its period and amplitude would grow with time. With the limited data available from this small study, we cannot specify which instability type causes the splitting of the streak. However, apparently similar modulations on similar hydrodynamic time scales have been observed before by means of optical probes and hence at different spatial resolution and lower plasma density [36].

In this paper we reported on the plasma reaction after *near-relativistic* pump laser irradiation of a thin wire. This study is limited to only a few shots, which means that we cannot give an estimate of the reproducibility. Additionally, the fits of the streak to obtain r are connected with large uncertainties and the fit of the surface expansion was not possible at all since the exponential roll-off due to the Debye–Waller factor was not visible (likely hidden in the background).

While absorption and phase contrast x-ray imaging [37] could also have been employed to visualize the dynamics of the bulk density on those scales, the spatial resolution of these methods is still limited to a few 100 nm and is thus larger than the relevant scales during or shortly after the laser pump irradiation itself—which is our future aim in order to eventually probe directly the early dynamics. For *ultra-relativistic* intensities, as they are relevant for many important applications such as ion acceleration, isochoric heating, or high harmonic generation, much faster and higher resolving probing is currently underdevelopment. The next generation of high intensity XFEL experiments are currently starting at European XFEL, using shorter probe pulses, larger detector distance and dynamic range, and background radiation suppression with chromatic mirrors. Then, the onset and early dynamics of the filamentation and plasma expansion could be studied and directly compared to existing models and particle-in-cell simulations.

Data availability statement

The data that support the findings of this study are openly available at the following URL/DOI: https://doi.org/10.14278/rodare.2146 [38].

Acknowledgments

This work was partially supported by DOE Office of Science, Fusion Energy Science under FWP 100182. Use of the Linac Coherent Light Source (LCLS), SLAC National Accelerator Laboratory, is supported by the U.S. Department of Energy, Office of Science, Office of Basic Energy Sciences under Contract No. DE-AC02-76SF00515. The experiments were performed at the Matter at Extreme Conditions (MEC) instrument of LCLS, supported by the DOE Office of Science, Fusion Energy Science under Contract No. SF00515. Christian Gutt acknoledges funding by DFG (GU 535/6-1). This work has also been supported by HIBEF (www.hibef.eu) and partially by H2020 Laserlab Europe V (PRISES) Contract No. 871124, and by the German Federal Ministry of Education and Research (BMBF) under Contract Number 03Z1O511.

ORCID iDs

Thomas Kluge https://orcid.org/0000-0003-4861-5584
Michael Bussmann https://orcid.org/0000-0002-8258-3881
Eric Galtier https://orcid.org/0000-0002-0396-285X
Siegfried Glenzer https://orcid.org/0000-0001-9112-0558
Christian Gutt https://orcid.org/0000-0002-0051-8542
Nicholas J Hartley https://orcid.org/0000-0002-6268-2436
Lingen Huang https://orcid.org/0000-0003-1184-2097
Alejandro Laso Garcia https://orcid.org/0000-0002-7671-0901
Emma E McBride https://orcid.org/0000-0002-8821-6126
Josefine Metzkes-Ng https://orcid.org/0000-0002-9556-0662
Motoaki Nakatsutsumi https://orcid.org/0000-0003-0868-4745
Irene Prencipe https://orcid.org/0000-0003-0931-1350
Martin Rehwald https://orcid.org/0000-0001-6200-6406
Toma Toncian https://orcid.org/0000-0001-7986-3631
Karl Zeil https://orcid.org/0000-0003-3926-409X
Ulrich Schramm https://orcid.org/0000-0003-0390-7671
Thomas E Cowan https://orcid.org/0000-0002-5845-000X

References

[1] Dalui M, Kundu M, Madhu Trivikram T, Ray K and Krishnamurthy M 2016 Manifestation of anharmonic resonance in the interaction of intense ultrashort laser pulses with microstructured targets *Phys. Plasmas* **23** 103101
Macchi A, Borghesi M and Passoni M 2013 Ion acceleration by superintense laser-plasma interaction *Rev. Mod. Phys.* **85** 751–93
Albert F *et al* 2021 2020 roadmap on plasma accelerators *New J. Phys.* **23** 031101
[2] Stark D J, Bhattacharjee C, Arefiev A V, Toncian T, Hazeltine R D and Mahajan S M 2015 Relativistic plasma polarizer: impact of temperature anisotropy on relativistic transparency *Phys. Rev. Lett.* **115** 025002
[3] Craxton R S *et al* 2015 Direct-drive inertial confinement fusion: a review *Phys. Plasmas* **22** 110501
[4] Sokolowski-Tinten K, Bialkowski J, Cavalleri A, Von der Linde D, Oparin A, Meyer-Ter-Vehn J and Anisimov S I 1998 Transient states of matter during short pulse laser ablation *Phys. Rev. Lett.* **81** 224
[5] Tatarakis M, Davies J R, Lee P, Norreys P A, Kassapakis N G, Beg F N, Bell A R, Haines M G and Dangor A E 1998 Plasma formation on the front and rear of plastic targets due to high-intensity laser-generated fast electrons *Phys. Rev. Lett.* **81** 999–1002
[6] Gremillet L *et al* 1999 Time-resolved observation of ultrahigh intensity laser-produced electron jets propagating through transparent solid targets *Phys. Rev. Lett.* **83** 5015–8
[7] Rehwald M *et al* 2023 Ultra-short pulse laser acceleration of protons to 80 MeV from cryogenic hydrogen jets tailored to near-critical density *Nat. Commun.* **14** 4009
[8] Geindre J P, Mysyrowicz A, Santos A D, Audebert P, Rousse A, Hamoniaux G, Antonetti A, Falliès F and Gauthier J C 1994 Frequency-domain interferometer for measuring the phase and amplitude of a femtosecond pulse probing a laser-produced plasma *Opt. Lett.* **19** 1997
Bocoum M, Böhle F, Vernier A, Jullien A, Faure J and Lopez-Martens R 2015 Spatial-domain interferometer for measuring plasma mirror expansion *Opt. Lett.* **40** 3009
[9] Mondal S, Lad A D, Ahmed S, Narayanan V, Pasley J, Rajeev P P, Robinson A P L and Kumar G R 2010 Doppler spectrometry for ultrafast temporal mapping of density dynamics in laser-induced plasmas *Phys. Rev. Lett.* **105** 105002
[10] Malvache A, Borot A, Quéré F and Lopez-Martens R 2013 Coherent wake emission spectroscopy as a probe of steep plasma density profiles *Phys. Rev.* E **87** 035101
[11] Hornung J, Zobus Y, Roeder S, Kleinschmidt A, Bertini D, Zepf M and Bagnoud V 2021 Time-resolved study of holeboring in realistic experimental conditions *Nat. Commun.* **12** 1–7
[12] Siders C W, Cavalleri A, Sokolowski-Tinten K, Toth C, Guo T, Kammler M, von Hoegen M H, Wilson K R, von der Linde D and Barty C P J 1999 Detection of nonthermal melting by ultrafast x-ray diffraction *Science* **286** 1340
[13] Sokolowski-Tinten K *et al* 2003 Femtosecond x-ray measurement of coherent lattice vibrations near the Lindemann stability limit *Nature* **422** 6929
[14] McBride E E *et al* 2019 Phase transition lowering in dynamically compressed silicon *Nat. Phys.* **15** 89–94
[15] Kluge T, Gutt C, Huang L G, Metzkes J, Schramm U, Bussmann M and Cowan T E 2014 Using x-ray free-electron lasers for probing of complex interaction dynamics of ultra-intense lasers with solid matter *Phys. Plasmas* **21** 033110

[16] Gorkhover T et al 2016 Femtosecond and nanometre visualization of structural dynamics in superheated nanoparticles *Nat. Photon.* **10** 93–97
[17] Kluge T et al 2018 Observation of ultrafast solid-density plasma dynamics using femtosecond x-ray pulses from a free-electron laser *Phys. Rev.* X **8** 031068
[18] Kluge T, Bussmann M, Chung H-K, Gutt C, Huang L G, Zacharias M, Schramm U and Cowan T E 2016 Nanoscale femtosecond imaging of transient hot solid density plasmas with elemental and charge state sensitivity using resonant coherent diffraction *Phys. Plasmas* **23** 033103
Kluge T et al 2017 Nanometer-scale characterization of laser-driven compression, shocks and phase transitions, by x-ray scattering using free electron lasers *Phys. Plasmas* **24** 102709
[19] Gaus L et al 2021 Probing ultrafast laser plasma processes inside solids with resonant small-angle x-ray scattering *Phys. Rev. Res.* **3** 043194
[20] Guinier A, Fournet G and Yudowitch K L 1955 *Small-angle Scattering of X-rays* (Wiley)
[21] Benedetti A, Fagherazzi G, Riello P, Zeng Y W, Pinna F and Signoretto M 1993 Fractal properties of a partially crystalline zirconium oxide aerogel *J. Appl. Crystallogr.* **26** 717–20
[22] Kluge T, Bussmann M, Schramm U and Cowan T E 2018 Simple scaling equations for electron spectra, currents and bulk heating in ultra-intense short-pulse laser-solid interaction *Phys. Plasmas* **25** 073106
[23] Mora P 2003 Plasma expansion into a vacuum *Phys. Rev. Lett.* **90** 185002
[24] Robinson A P L, Gibbon P, Zepf M, Kar S, Evans R G and Bellei C 2009 Relativistically correct hole-boring and ion acceleration by circularly polarized laser pulses *Plasma Phys. Control. Fusion* **51** 024004
[25] Fiuza F, Fonseca R A, Tonge J, Mori W B and Silva L O 2012 Weibel-instability-mediated collisionless shocks in the laboratory with ultraintense lasers *Phys. Rev. Lett.* **108** 1–5
[26] Santos J J et al 2017 Isochoric heating and strong blast wave formation driven by fast electrons in solid-density targets *New J. Phys.* **19** 103005
[27] Bulgakova N M 1999 Possibility of rarefaction shock wave under short pulse laser ablation of solids *Phys. Rev.* E **60** R3498–500
[28] Palmer C A J et al 2012 Rayleigh-Taylor instability of an ultrathin foil accelerated by the radiation pressure of an intense laser *Phys. Rev. Lett.* **108** 225002
[29] Sgattoni A, Sinigardi S, Fedeli L, Pegoraro F and Macchi A 2015 Laser-driven Rayleigh-Taylor instability: plasmonic effects and three-dimensional structures *Phys. Rev.* E **91** 013106
[30] Kluge T, Metzkes J, Zeil K, Bussmann M, Schramm U and Cowan T E 2015 Two surface plasmon decay of plasma oscillations *Phys. Plasmas* **22** 64502
[31] Bret A, Firpo M C and Deutsch C 2004 Collective electromagnetic modes for beam-plasma interaction in the whole [Formula presented] space *Phys. Rev.* E **70** 15
[32] Metzkes J, Kluge T, Zeil K, Bussmann M, Kraft S D, Cowan T E and Schramm U 2014 Experimental observation of transverse modulations in laser-driven proton beams *New J. Phys.* **16** 23008
[33] Göde S et al 2017 Relativistic electron streaming instabilities modulate proton beams accelerated in laser-plasma interactions *Phys. Rev. Lett.* **118** 194801
[34] Quinn K et al 2012 Weibel-induced filamentation during an ultrafast laser-driven plasma expansion *Phys. Rev. Lett.* **108** 135001
[35] Beg F N et al 2004 High-intensity-laser-driven Z-pinches *Phys. Rev. Lett.* **92** 095001
[36] Rehwald M 2022 *Laser-Proton Acceleration in the Near-Critical Regime Using Density Tailored Cryogenic Hydrogen Jets* (Helmholtz-Zentrum Dresden - Rossendorf)
[37] Schropp A et al 2015 Imaging shock waves in diamond with both high temporal and spatial resolution at an XFEL *Sci. Rep.* **5** 11089
[38] Raw data for: Probing shock dynamics inside micro-wire targets after high-intensity laser irradiation using small angle x-ray scattering of a free-electron laser (repository name: rodare) (https://doi.org/10.14278/rodare/2146)